



Research article

Evading the strength-ductility trade-off dilemma in AA2024 alloy by short-term natural re-aging after T351 temper

Farima Haghdadi, Roohollah Jamaati^{*}, Seyed Jamal Hosseinipour*Department of Materials Engineering, Babol Noshirvani University of Technology, Shariati Ave, Babol, 47148-71167, Iran*

ARTICLE INFO

Keywords:AA2024 alloy
Natural aging
Microstructural evolution
Mechanical behavior

ABSTRACT

In this research, the influence of short-term natural re-aging after T351 temper on the microstructural evolution and mechanical behavior of AA2024 aluminum alloy was investigated. Grain growth occurred in the microstructures of the natural re-aged sample and a large number of $\text{Al}_7\text{Cu}_2\text{Fe}$ particles were located inside the alpha grains. At the re-aging time of 1440 min, the peaks of XRD were shifted strongly to the right due to the formation of θ'' , S'' , θ' , and S' . The results revealed that the precipitation rate was high in the AA2024 alloy during natural aging. With increasing the re-aging time, texture parameters remained almost unchanged. The hardness increased slowly within the first 60 min, then enhanced rapidly between 60 and 2880 min, and finally became stable at around 139 HV between 2880 and 11520 min. When the natural re-aging time increased from 240 to 2880 min, the strengthening trended speed up, viz, the yield strength increased from 226.6 to 357.3 MPa, and the ultimate tensile strength enhanced from 452.2 to 535.5 MPa. Compared to the as-received sample (T351 temper), the ultimate tensile strength of the re-aged sheet improved from 455.5 to 535.5 MPa, the ductility remained unchanged, and the hardness increased from 128.8 to 138.2 HV, which was owing to the acceleration of the precipitation caused by the presence of high-content $\text{Al}_7\text{Cu}_2\text{Fe}$ particles in the interior of the alpha-aluminum grains in the natural re-aged sample. It was found that the Portevin-Le Chatelier instability of AA2024 alloy was effectively postponed after natural re-aging. With increasing the natural re-aging time, the strain hardening rate of the AA2024 sheet increased. The strengthening of the natural re-aged sample for 1440 and 2880 min was a result of a synergistic effect of precipitation hardening due to the formation of θ'' , S'' , θ' , and S' phases, elimination of Portevin Le-Chatelier instability, and highly efficient load transfer from alpha-aluminum to $\text{Al}_7\text{Cu}_2\text{Fe}$. Finally, to use the A2024 alloy produced by natural re-aging for 1440 or 2880 min, two methods were proposed.

1. Introduction

Heat-treatable AA2024 aluminum alloy is intensively used in military, aerospace, and automotive industries due to its good corrosion resistance, high strength/density ratio, and good fatigue resistance [1–5]. In the AA2024 alloy, the mechanical properties mainly originate from metastable precipitates formed during aging treatment. The general precipitation sequences of AA2024 alloy are [6–9]:

^{*} Corresponding author.

E-mail address: jamaati@nit.ac.ir (R. Jamaati).

<https://doi.org/10.1016/j.heliyon.2024.e27257>

Received 11 January 2024; Received in revised form 27 February 2024; Accepted 27 February 2024

Available online 2 March 2024

2405-8440/© 2024 The Authors. Published by Elsevier Ltd. This is an open access article under the CC BY-NC-ND license (<http://creativecommons.org/licenses/by-nc-nd/4.0/>).

1. Supersaturated solid-solution \rightarrow Guinier-Preston (GP) zones $\rightarrow \theta'' \rightarrow \theta' \rightarrow \theta$ (Al₂Cu)
2. Supersaturated solid-solution \rightarrow Guinier-Preston-Bagaryatsky (GPB) zones $\rightarrow S'' \rightarrow S' \rightarrow S$ (Al₂CuMg)

Although the AA2024 alloy has been known for several decades, the mechanisms underlying the formation of precipitates during natural and artificial aging treatment are still the subject of many research works. AA2024 alloy has high strength after artificial aging but it is too brittle to plastically deform in this state. However, during a very short time after solution heat treatment followed by quenching, this alloy reveals high ductility and low strength. In fact, the initial stages of natural aging are the best state to perform final cold forming such as cold stamping. Therefore, it is demanded to develop AA2024 alloy with high ductility by natural aging. Meanwhile, the naturally aged AA2024 alloy should have enough strength to meet service requirements.

Despite considerable studies devoted to investigating the precipitation behavior in the AA2024 alloy during artificial aging treatment, the works on the natural aging of this alloy have been so far limited. Lotter et al. [10] investigated the natural ageing of Al–Cu–Mg and Al–Cu alloys. Based on this research, the Al–Cu–Mg sheet exhibited a remarkably enhanced hardening response compared to the Al–Cu sample owing to the different compositions of the clusters generated during natural aging. Kim et al. [11] studied the effect of natural + artificial aging treatments and magnesium atoms on the clustering behavior of aluminum-copper alloy. The growth of clusters during aging treatment at room temperature was rarely influenced, even though the chemical composition of the clusters was changed by the content of magnesium. They reported that clusters created during aging treatment at room temperature partially dissolved during subsequent artificial aging treatment. Klobes et al. [2] investigated the natural aging of AA2024 alloy. They reported that during natural aging the chemical environment of vacancies is generated for both copper and magnesium atoms. Also, the rearrangement of vacancy surroundings led to an enhancement in the hardness of AA2024 alloy. Copper atoms were embedded near the vacancies and therefore the vacancies were gently trapped inside the clusters. Ivanov et al. [12] studied the kinetics of clustering during the natural ageing of Al–Cu–Mg. When the magnesium/copper ratio of the alloy was high, magnesium atoms quickly clustered with the initial copper-rich domains leading to an improvement in the hardness value owing to the formation of strong copper-magnesium bonds. Liu et al. [13] investigated the influence of high-pressure torsion followed by natural aging on the tensile behavior of AA2024 alloy. A hierarchical nanostructured was produced by high-pressure torsion and natural aging. The triple strengthening effects including the S'/S precipitates, the secondary phase (oxide particles) hardening, and the grain refinement led to a high yield strength (YS) and tensile strength (UTS) of 934 and 992 MPa, respectively. However, the ductility significantly decreased to 2%. Österreicher et al. [14] investigated the effect of secondary aging on the formability of an AA2024 sheet in W and under-aged tempers. The pre-aged temper was stronger than the W one at the early stages of natural aging. However, further natural aging was effectively suppressed, and after 24 h, the strength was lower than the W temper naturally aged for the same time. Also, the formability of the pre-aged AA2024 sheet was slightly larger. They stated that the generation of GPB zones and S decreases the driving force for magnesium/copper co-cluster precipitation during secondary natural aging. Therefore, the improvement of strength associated with natural aging was inhibited. It should be noted that in industrial production, natural aging is inevitable in the AA2024 sheet due to the delay between the quenching and final forming process. Therefore, it is worthwhile to investigate the natural aging of the AA2024 sheet to achieve high strength-ductility balance (toughness).

T6 temper is an important temper for the AA2024 alloy for aerospace applications. This temper includes solution heat-treated, then artificially aged. Recently, the application of T6 for AA2024 has been limited by technical issues such as the high cost of processing (due to long-term artificial aging treatment) [15]. The motivation of the current study is to achieve a higher toughness than T6 temper in AA2024 alloy concurrently with high ductility, without PLC instability by short-term natural re-aging after T351 temper as a new technique to conventional T6 procedure. There is no published work about the natural re-aging of AA2024 alloy in the literature. The present research explores the precipitation hardening, mechanical properties, PLC instability, and work-hardening behavior during natural re-aging at different times in the AA2024 alloy.

2. Materials and methods

The investigated material was an AA2024 alloy sheet with a thickness of 2 mm. The chemical composition and mechanical properties of the as-received sheet are given in Tables 1 and 2, respectively. The temper of the as-received AA2024 was T351 (solution heat-treated, stress relieved by 2% stretching, then naturally aged). The initial sheets were solutionized at 500 °C for 60 min and then water-quenched. The quenched samples were naturally re-aged at ambient temperature for different times up to 11520 min (8 days).

Optical microscope (OM), scanning electron microscope (SEM), and transmission electron microscope (TEM) under a voltage of 300 kV were utilized to characterize the microstructure, precipitates, and fracture surfaces of the sheets. TEM samples were prepared using grinding to a thickness of 50 μm and jet-polishing at –30 °C by an electrolyte consisting of 67 vol % CH₃OH + 33 vol % HNO₃. The quantitative analysis was conducted by Image J software.

The samples at different stages of the natural aging were ground and polished to a mirror finish using standard metallography procedures for Vickers hardness tests with a load of 100 g and a dwell time of 10 s. The mean value of nine points was determined to

Table 1
The alloy composition of the as-received sheet (wt.%).

Cu	Mg	Mn	Fe	Si	Zn	Ti	Al
4.90	1.43	0.66	0.28	0.21	0.06	0.04	Bal.

Table 2
Mechanical properties of the as-received sheet.

YS (MPa)	UTS (MPa)	Ductility (%)	Hardness (HV)
351.6	455.5	28.8	128.8

avoid unexpected errors during the hardness test. The error bars were achieved by calculation of standard deviation. The hardness measurements obtained within 5 min after the quenching correspond to the as-quenched condition (0 min). The uniaxial tensile tests of the samples were conducted on a Santam tensile device at ambient temperature. The testing was conducted at a crosshead speed of 1 mm per minute. The length and width of the gauge were 12 and 3 mm, respectively.

3. Results and discussion

The RD-TD and RD-ND microstructures of the as-received AA2024-T351 sheet are depicted in Fig. 1(a–d). The microstructure consists of coarse alpha-aluminum grains with a mean grain size of 33.1 μm on the RD-TD section, elongated alpha grains with an average width of 13.2 μm on the RD-ND section, and hard and brittle intermetallic compound particles. These intermetallic compounds are mainly ω - $\text{Al}_7\text{Cu}_2\text{Fe}$, which will be confirmed by X-ray analysis. The $\text{Al}_7\text{Cu}_2\text{Fe}$ phase is formed during the solidification of AA2024 alloy. Based on the quantitative analysis, the volume fraction of these particles in the as-received alloy is about 3%. In the as-received sheet, due to rolling (before T351 temper), the grains are elongated along the rolling direction. The important question is why, despite the solution heat treatment during T351 temper and dissolution of precipitates, the grains are still elongated and do not become equiaxed grains in the RD-ND plane of the sheet. During the production of this alloy by rolling (before T351 temper), $\text{Al}_7\text{Cu}_2\text{Fe}$ intermetallic compounds fragmented along the direction of rolling as displayed by blue arrows in Fig. 1(b) and (d). This creates obstacles (finer $\text{Al}_7\text{Cu}_2\text{Fe}$ particles) for the migration of grain boundary (during solution heat treatment of T351 temper) in the direction of fragmented particles. Based on Zener pinning, fine particles can act to inhibit the motion of grain boundaries by exerting a pinning pressure which counteracts the driving force pushing the grain boundaries [16–18]. Therefore, the grain growth towards the rolling direction remains without hindrance, while, fine $\text{Al}_7\text{Cu}_2\text{Fe}$ particles inhibit the grain growth in the normal direction of the sheet. Consequently, the elongated shape of the grains is preserved as observed in Fig. 1(c) and (d).

The RD-TD and RD-ND microstructures of the natural re-aged sample are demonstrated in Fig. 2(a–d). It is clear that grain growth has occurred in the microstructures of the natural re-aged sample. The average grain size of the RD-TD plane is 54.5 μm and the

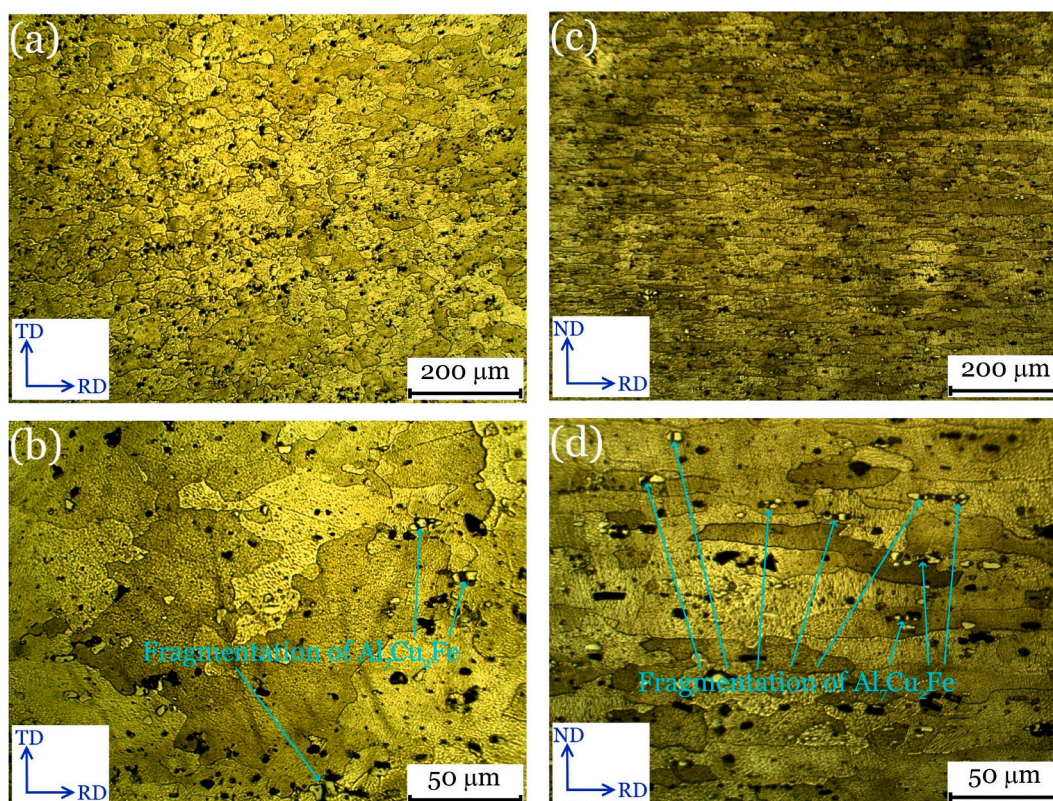


Fig. 1. The microstructures of the as-received (T351) sample.

average grain width of the RD-ND plane is 19.3 μm . The grain growth is due to secondary solution heat treatment. Increasing the grain width from 13.2 to 19.3 μm (46% increase) indicates that grain growth has occurred even in the normal direction of the sheet. This grain growth during solution heat treatment may be effective in the precipitation behavior of the AA2024 alloy during re-aging treatment, which will be investigated further. From Fig. 1, the $\text{Al}_7\text{Cu}_2\text{Fe}$ particles are mainly located in the grain boundaries. However, Fig. 2 shows that a large number of grain boundaries have passed through the $\text{Al}_7\text{Cu}_2\text{Fe}$ particles as a result of secondary solution treatment. Therefore, a large number of $\text{Al}_7\text{Cu}_2\text{Fe}$ particles are placed inside the alpha grains.

Fig. 3 depicts the XRD profiles of the natural re-aged samples at different times. The (111), (200), (220), and (311) peaks of the alpha-aluminum phase can be observed in Fig. 3(a). These patterns, do not show any peak that could be attributed to Al_2Cu (θ) precipitates in the re-aged samples, indicating that the content of the θ precipitates is insufficient to show a peak. There were several peaks of the insoluble $\text{Al}_7\text{Cu}_2\text{Fe}$ intermetallic particles that were marked with triangles in Fig. 3(a). To clearly show the change of the peak shifting with re-aging time, the (200) peak of all samples is magnified and depicted in Fig. 3(b). The enlarged diffraction profiles show important changes. By increasing the re-aging time to 240 min, there is no shift in the peak. This result shows that until 240 min, the precipitation progresses only to the generation of GP and GPB zones, because, in the precipitation sequence of the AA2024 alloy, the lowest coherency strain belongs to the GP and GPB zones. In the early stages of aging (up to 240 min), copper clusters have the same crystal structure as the host aluminum matrix, showing no interface. Therefore, the coherency is high and there is no lattice distortion. According to Fig. 3(b), at the re-aging time of 1440 min, the peak has shifted strongly to the right. This can be attributed to the formation of θ'' , S'' , θ' , and S' during natural re-aging which is accompanied by the formation of coherent (not fully coherent) and semi-coherent interfaces. This creates high coherency strains and causes severe lattice distortion in the unit cells of aluminum near the precipitates. From Fig. 3(b), by further increasing the re-aging time to 2880 min, the value of peak shifting decreases due to the formation of more θ and S with incoherent interfaces in the AA2024 alloy. The formation of the θ and S can consume solute copper and magnesium atoms and produce incoherent interfaces with low coherency strains. Therefore, the lattice distortion of alpha-aluminum is decreased, and the peak shifting is reduced, which is in line with the previous works [19,20]. With a further increase in the re-aging time to 5760 and 11520 min, the amount of peak shifting is almost unchanged.

To prove the formation of θ'' , S'' , θ' , and S' precipitates during the natural aging time of 1440 min, the high-resolution TEM image of this sample is shown in Fig. 4 θ'' and S'' are multilayered precipitates, and θ' and S' are thick precipitates [11,21,22]. After 1440 min of natural re-aging time, the coexistence of θ'' , S'' , θ' , and S' phases is observed in the alpha-aluminum matrix of the AA2024 alloy. Comparably, there are more S'' and S' and fewer θ'' and θ' precipitates in the re-aged sample for 1440 min. This is due to the presence of a considerable content of magnesium atoms (1.43 wt%) in the as-received alloy which was obtained via quantum analysis. It is reasonable that, at room temperature, the thermodynamic driving force is not high enough to develop high-content and larger θ'' , S'' , θ' ,

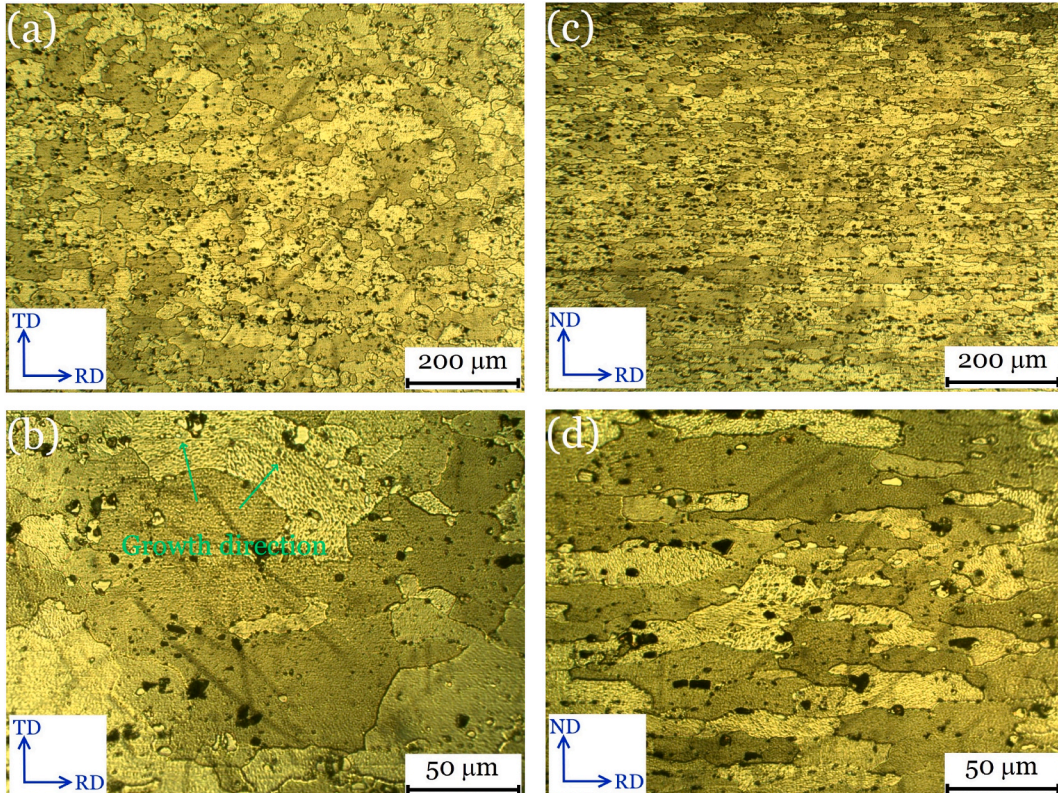


Fig. 2. The microstructures of the natural re-aged sheet.

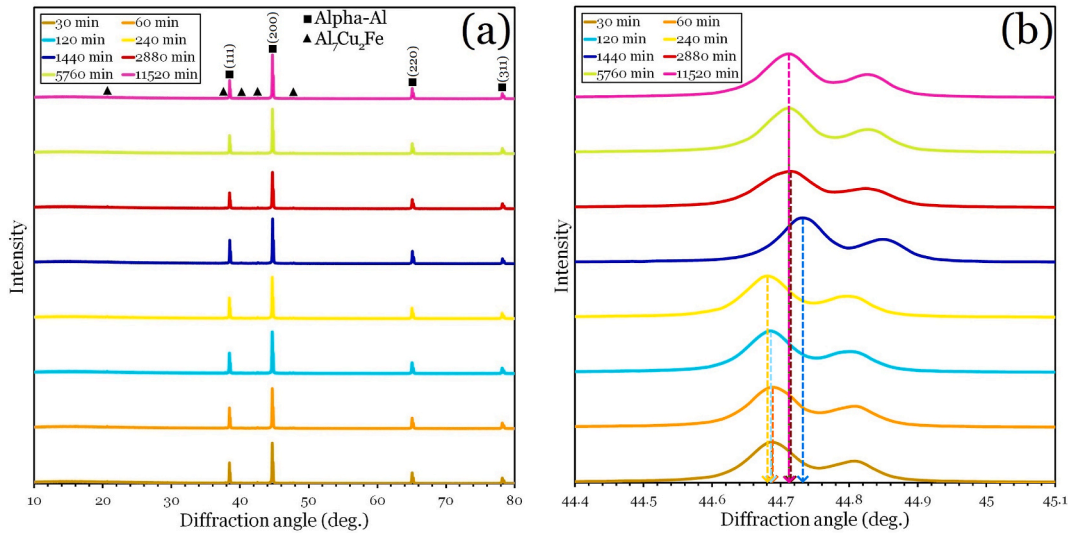


Fig. 3. (a) The XRD profiles of the natural re-aged samples at different times. (b) The enlarged diffraction profiles of (200) peak.

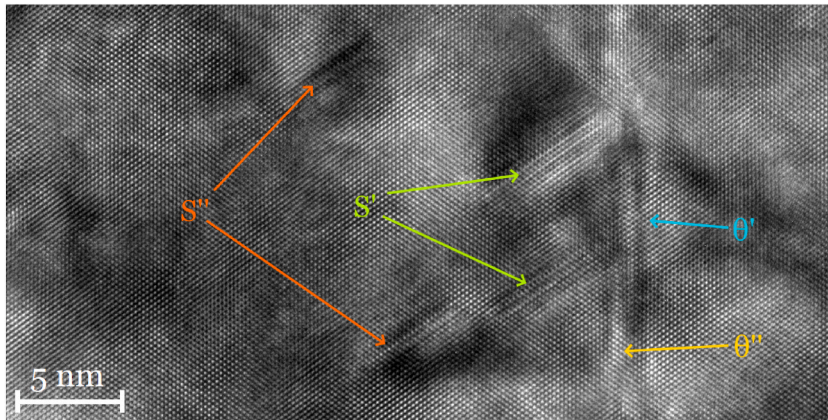


Fig. 4. The HRTEM of the microstructure of the sample after 1440 min of natural re-aging treatment.

and S' precipitates. From Fig. 4, the precipitation of θ and S cannot be observed. Despite aging at ambient temperature, the precipitation rate was high in the present work. This indicates that there are more sites for the nucleation of precipitates in this study. Based on the results above, there are three possible reasons.

1. This result can be ascribed to the presence of considerable magnesium content in the as-received sheet. It was reported that the presence of magnesium atoms remarkably increases the response to natural aging [12,20–22]. Ivanov et al. [12] indicated a considerable acceleration of clustering in the Al–Cu–Mg sheet brought by the presence of magnesium atoms. The presence of magnesium atoms is important for the initial formation of copper clusters since, in the absence of magnesium atoms, copper clustering barely happens. In the Al–Cu–Mg sheets, the clustering initially proceeds by copper atoms and then the formation of copper-magnesium-rich clusters [12]. The precipitation of the copper-rich GP zone can be accelerated owing to these copper-magnesium-rich clusters which form additional sites and decrease the activation energy for the nucleation of the GP zone [23,24].
2. The coefficient of thermal expansion values for the alpha-aluminum and Al_7Cu_2Fe phases are $25.5 \times 10^{-6} K^{-1}$ [23] and $8.5 \times 10^{-6} K^{-1}$ [24], respectively. Therefore, during the water-quenching, a high density of dislocations can be produced in the alpha-aluminum owing to the large mismatch in the thermal expansion coefficient between the alpha-aluminum and Al_7Cu_2Fe phases. This increases the diffusion rate of copper and Mg atoms and decreases the activation energy for heterogeneous nucleation of precipitates during the aging treatment. According to Figs. 1 and 2, the Al_7Cu_2Fe particles in the interior of the alpha grains of the re-aged sample were more than that of the T351 sample. The presence of particles in the interior of the grains (in the re-aged sample) generated more dislocations compared to the presence of particles at the grain boundaries of the alpha phase (in the T351 sample). Therefore, the presence of Al_7Cu_2Fe particles in the interior of the alpha grains can accelerate the precipitation

behavior of the AA2024 alloy. According to previous research, Al_7Cu_2Fe particles can be characterized as heterogeneous nucleation sites for the precipitates [25–27].

3. According to the microstructures (Figs. 1 and 2) and also the XRD patterns (Fig. 3), a high content of Al_7Cu_2Fe particles has existed in the AA2024 alloy. The high content of particles in the alloy provides more diffusion paths for the copper and magnesium atoms [27], which can contribute to accelerated precipitation. In addition, the presence of a high content of Al_7Cu_2Fe particles generates more dislocations in the vicinity of the Al_7Cu_2Fe /aluminum interfaces, which enhances the diffusion of copper and magnesium atoms, and consequently promotes the nucleation of precipitates and accelerates the precipitation.

According to Fig. 3(a), the intensity of diffraction peaks almost remained unchanged at different times of natural re-aging. In other words, increasing the aging time caused no variation in the characteristic peak intensity of the alpha-aluminum phase. This means that the grain orientation does not change during natural re-aging. For a more detailed analysis of this issue, the texture parameters of the (111), (200), (220), and (311) planes of the natural re-aged samples were calculated and are depicted in Fig. 5. As seen in Fig. 5, the samples exhibit a strong $\langle 100 \rangle \parallel ND$ (θ -fiber) texture, a moderate $\langle 110 \rangle \parallel ND$ (α -fiber) texture, and a weak $\langle 111 \rangle \parallel ND$ (γ -fiber) texture. With increasing the re-aging time from 30 min to 11520 min, texture parameters of the (111), (200), (220), and (311) planes remained almost constant. The creation of GP and GPB zones and precipitates during re-aging treatment cannot cause the grains to rotate and change the texture of the samples. Therefore, the crystallographic texture will not have any effect on the differences in the mechanical properties of the samples.

Fig. 6 shows the Vickers hardness of the samples during natural re-aging treatment. It can be observed that after an initial short plateau, the hardness of the AA2024 sheet tends to enhance gradually during natural re-aging treatment. The hardness of the AA2024 sheet increases slowly within the first 60 min due to the generation of GP and GPB zones, then enhances rapidly between 60 min and 2880 min owing to the formation of precipitates, and finally becomes stable at around 139 HV between 2880 min and 11520 min. The hardness evolution during natural re-aging reveals an enhanced hardness increase with aging time. Stored at room temperature after secondary solution treatment followed by water-quenching has resulted in a 48% hardness improvement in the AA2024 alloy. In previous work, during the natural aging of the AA2024 sheet, a maximum (saturation) hardness of ~ 120 HV was achieved after 2 days (2880 min) and further increasing the time of natural aging did not affect the hardness of the alloy [12]. According to Fig. 6, the saturation hardness is about 139 HV which was obtained after 2880 min natural re-aging. This can be attributed to performing the natural re-aging in the present work. As seen in Table 2, the hardness of the as-received AA2024-T351 sheet was 128.8 HV, while the final hardness of the natural re-aged sample was 139.0 HV. As mentioned before, the presence of more Al_7Cu_2Fe particles in the interior of the alpha grains in the re-aged sample compared to the T351 sample can accelerate the precipitation behavior of the AA2024 alloy [17]. Therefore, the hardness of the re-aged sample is larger than that of the as-received T351 sheet.

The stress-strain curves of the natural re-aged sheets are depicted in Fig. 7. Also, Fig. 8(a–d) displays the evolutions of YS, UTS, ductility, and toughness with the natural re-aging time of samples. The as-quenched sheet exhibits a low yield strength of 180.2 MPa, moderate tensile strength of 432.0 MPa, high ductility of 31.1%, and moderate toughness of 111.7 J cm^{-3} . At the early stages of natural aging (up to 30 min), the yield and tensile strength slightly decreased to 165.5 MPa and 400.8 MPa, respectively, while the ductility slightly increased to 33.1%. This can be ascribed to the presence of Cu atoms in the boundaries at the early stages of natural aging. It was reported that the presence of Cu atoms in the boundaries of alpha-aluminum increases the strength of the grain boundary [28]. The presence of copper atoms in the grain boundaries enhances the charge density of boundaries and forms new bonds with the surrounding aluminum atoms, which improves the strength of grain boundaries [28]. The strength of the grain boundary reduced with a

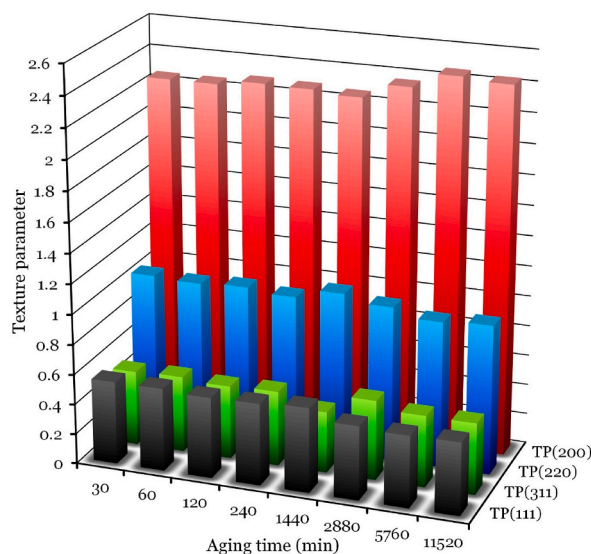


Fig. 5. The texture parameters of the (111), (200), (220), and (311) planes of the natural re-aged samples.

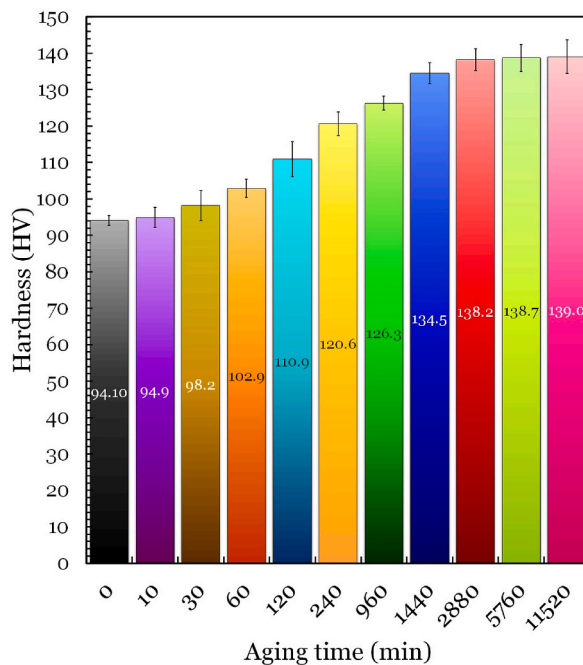


Fig. 6. The Vickers hardness as a function of natural re-aging duration.

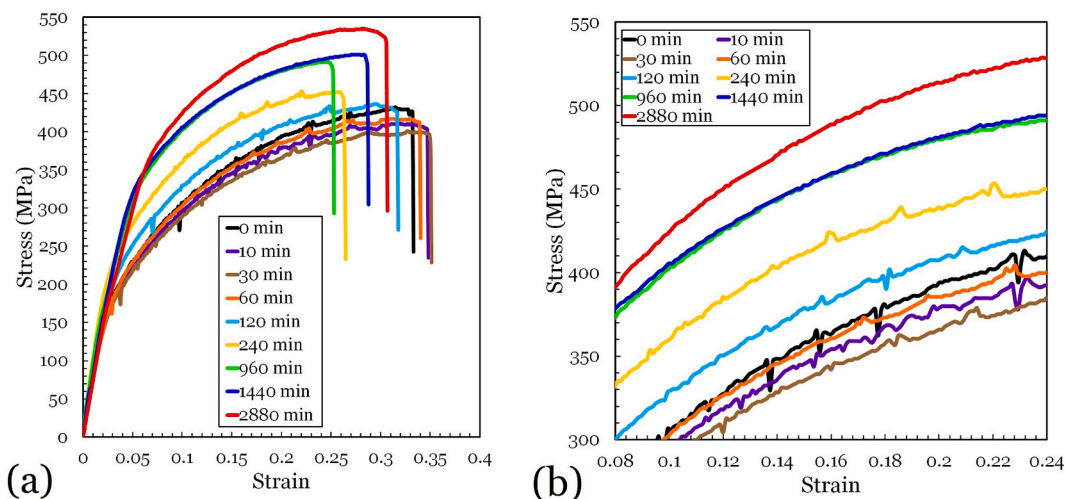


Fig. 7. Tensile deformation behaviors of the AA2024 sheet after different times of natural re-aging. (a) Stress-strain curves and (b) local magnification of curves.

reduction in the copper concentration. By increasing the natural aging time to 30 min, the number of Cu atoms in the boundaries decreases due to the diffusion of copper into the alpha grains. Therefore, the strength of the AA2024 sheet decreases, and its ductility increases. It should be noted that until 30 min of natural aging, the GP and GPB zones have not yet been formed so that they can prevent the reduction of the strength of the sample, which is caused by the reduction of the strength of the grain boundaries. With a further increase in aging time up to 960 min, owing to the formation of GP and GPB zones, the strength and ductility show an increasing and decreasing trend, respectively.

When the natural re-aging time increases from 240 min to 2880 min, the strengthening trends speed up, viz, the yield strength increases from 226.6 to 357.3 MPa and the ultimate tensile strength increases from 452.2 to 535.5 MPa. With increasing the re-aging time from 960 to 2880 min, the ductility improves from 22.9% to 28.9% and toughness is enhanced from 97.8 to 131.0 J cm⁻³. Increasing the ductility of the AA2024 alloy after 1440 and 2880 min of natural re-aging can be attributed to the significant weakening of the Portevin-Le Chatelier instability and higher strain hardening which will be discussed later.

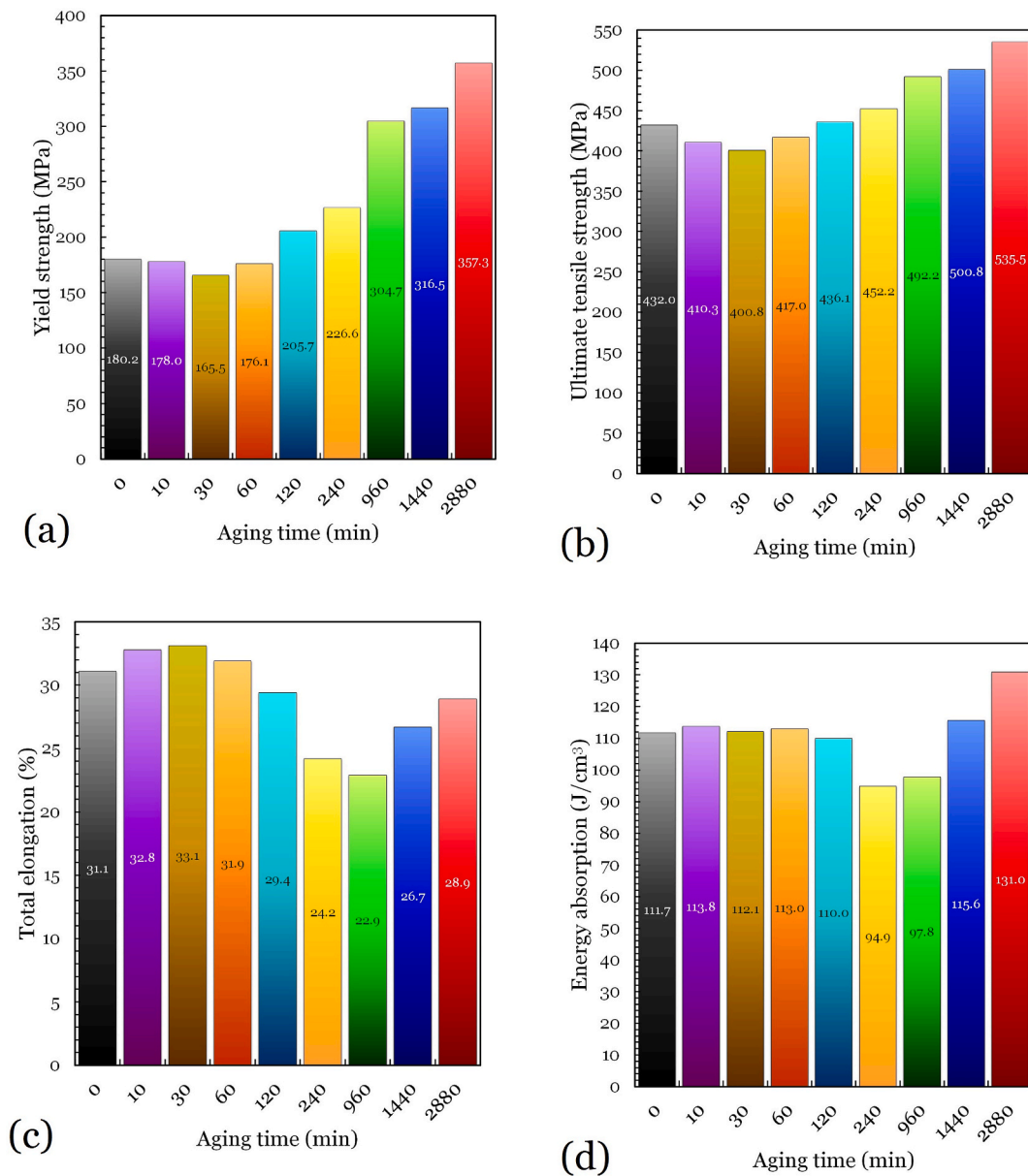


Fig. 8. The variations of (a) YS, (b) UTS, (c) ductility, and (d) toughness of the natural re-aged samples.

Compared to the as-quenched sheet, the strength of the AA2024 sheet rapidly improved within 2880 min, that is, the yield strength significantly increased from 180.2 to 357.3 MPa (98% improvement), the ultimate tensile strength increased from 432.0 to 535.5 MPa (24% improvement), and the ductility slightly decreased from 31.1% to 28.9%. These results indicate that the AA2024 sheet has a superior strengthening response to natural re-aging. This strengthening is mainly attributed to the formation of precipitates during natural re-aging treatment.

Compared to the as-received sample (T351 temper), the yield strength of AA2024 sheet after 2880 min natural re-aging improved from 351.6 to 357.3 MPa, the ultimate tensile strength enhanced from 455.5 to 535.5 MPa, the ductility remained unchanged, and the hardness increased from 128.8 to 138.2 HV. According to microstructural observations, such enhancements in hardness and tensile properties of the AA2024 alloy can be mainly ascribed to the acceleration of the precipitation due to the presence of high-content $\text{Al}_7\text{Cu}_2\text{Fe}$ particles in the interior of the alpha-aluminum grains in the natural re-aged sample compared to the T351 sample. These results demonstrated that the natural re-aging would significantly affect the mechanical properties of AA2024-T351 alloy. A superb combination of strength and ductility is achieved for the natural re-aged sample for 1440 and 2880 min. It is worthwhile mentioning that this superior strength-ductility balance is obtained by only a natural re-aging treatment without the performing long-term artificial aging or the application of plastic deformation techniques such as rolling and extrusion.

Fig. 7(b) depicts the corresponding local magnification of the stress-strain curves of the AA2024 sheet after different times of natural re-aging. Portevin-Le Chatelier instability (serrations) can be seen in the stress-strain curves of all samples. From the literature [29,30], there are three different types of Portevin-Le Chatelier instability based on the propagation characteristics. In type A, the serrations propagate without interruption and the curve demonstrates periodic fluctuation. In type B, the serrations propagate discontinuously and the curve oscillates. In type C, the serrations nucleate randomly and the curve drops. Fig. 7(b) indicates that, up to 240 min natural re-aging, the serrations propagate discontinuously, which means that the Portevin-Le Chatelier instability of these samples belongs to type B. However, with further increasing the natural re-aging, the propagation of the serrations is different. The Portevin-Le Chatelier instability of the samples after 960, 1440, and 2880 min of natural re-aging propagated continuously. Therefore, it can be concluded that with increasing the natural re-aging time, the feature of the serrations is changed from type B (natural re-aging time ≤ 240 min) to type A (natural re-aging time ≥ 960 min). During natural re-aging, the reduction in the content of copper and magnesium solutes decreases the number of pinned dislocations, which changes the feature of the Portevin-Le Chatelier instability from type B to type A, which can be supported by previous works [29,31]. They indicated that the number of pinned dislocations is effective on the feature of the Portevin-Le Chatelier instability.

To further understand the effect of natural re-aging on the Portevin-Le Chatelier instability, the magnitude of stress drops is

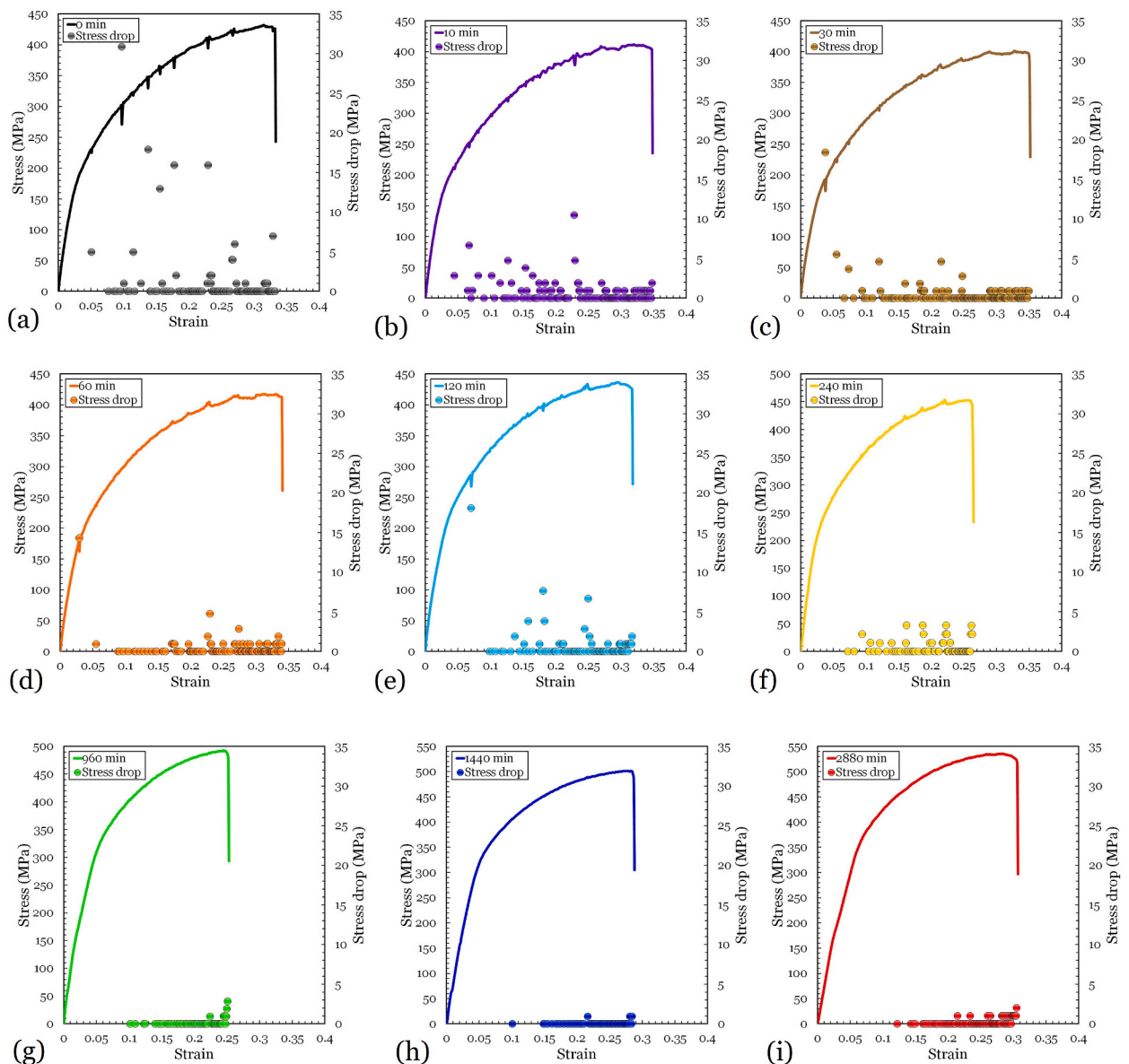


Fig. 9. The flow curves and stress drop of the AA2024 sheet after (a) 0, (b) 10, (c) 30, (d) 60, (e) 120, (f) 240, (g) 960, (h) 1440, and (i) 2880 min natural re-aging.

calculated and demonstrated in Fig. 9. Also, the mean amplitude of stress drop and critical strain of all samples are shown in Fig. 10. It should be noted that the mean amplitude of the stress drop shows the intensity of hindrance of dissolved atoms against the movement of dislocations. The critical strain of stress drop demonstrates the initiation of the dislocation pinning [29,32]. As seen in Figs. 9 and 10, the average amplitude of stress drop of the natural re-aged sheets is in the range of 1–6 MPa. It can be observed that the stress drop amplitude is highest in the as-quenched sample. During the tensile test, a significant Portevin-Le Chatelier instability is seen in the as-quenched sheet. The amplitude of stress drop is high for the re-aging times up to 240 min. With further increasing the natural re-aging time, the amplitude of stress drop is significantly decreased owing to the creation of precipitates. At the as-quenched state, the average amplitude of stress drop is 5.65 MPa, while this value after 2880 min of natural re-aging decreased to 1.06 MPa (81% reduction in average amplitude). The value of the critical strain is another important feature of Portevin-Le Chatelier instability. This value first decreases from 0.051 to 0.029 by increasing the re-aging time from 0 to 60 min. Diffusion of copper and magnesium atoms from the grain boundaries to the interior of the grains in the early stages of natural re-aging can lead to an increase in the probability of dislocation interaction with these atoms at low strains. As a result, the amount of critical strain is reduced. The critical strain increases gradually from 0.029 to 0.122 with increasing the natural re-aging time from 60 to 2880 min. This is due to the formation of GP, GPB, and precipitates after 60 min of natural re-aging time. This result shows that the serrations of AA2024 alloy are effectively postponed after natural re-aging. The serrations in the stress-strain curve of the sheets after 960, 1440, and 2880 min have almost disappeared. It shows that the content of solute copper and Mg atoms in the alpha-aluminum has been greatly reduced due to the formation of precipitates. In other words, the formation of precipitates consumes solute copper and magnesium atoms, leading to the suppression of Portevin-Le Chatelier instability during tensile deformation. The suppression of Portevin-Le Chatelier instability can increase the alloy's ductility as reported in previous works [22,33,34]. For this reason, the ductility of the samples after 1440 and 2880 min of natural re-aging was enhanced (see Fig. 7(a) and 8(c)).

To investigate the work hardening behavior, the work hardening rate ($\theta = d\sigma/d\varepsilon$) of the samples after different natural re-aging times is plotted against true strain (Fig. 11(a–d)). Note that no fitting and smoothing of the curves was performed to observe the serrations. The natural re-aging time appears to have a strong impact on the strain-hardening rate of the AA2024 sheet. As seen, the strain hardening rate curves demonstrate a steep drop from an initial large hardening rate due to the elastic-plastic transition. Portevin-Le Chatelier instability led to very sharp fluctuations in the work hardening rate curve. It is clear that the Portevin-Le Chatelier instability decreases drastically with increasing natural re-aging time, which can have a positive effect on the ductility and toughness of the AA2024 alloy. This is in accordance with the findings reported by Lee et al. [35]. As seen in Fig. 11(d), the work hardening curve of the as-quenched sheet lies at the lower left corner and is indicative of lower strain hardening capability. At the natural re-aging of 2880 min, the strain hardening curve shifts right and upwards indicating an enhancement in work hardening behavior at the longer aging time. In other words, with increasing the natural re-aging time, the strain hardening rate of the AA2024 sheet is increased. The large work hardening rate after the natural re-aging time of 1440 and 2880 min can be explained by a large number of coherent and semi-coherent precipitates that interact with dislocations as reported by Liu et al. [36]. Consequently, the capacity of dislocations to be accumulated in the interior of alpha grains is enhanced, resulting in high ductility. It can be concluded that the high work hardening is responsible for the increase in ductility and formability of the re-aged samples for 1440 and 2880 min, resulting in improved toughness of the AA2024 alloy as displayed in Fig. 8.

Fig. 12(a–h) depicts the SEM micrographs of fracture morphology of the natural re-aged samples for 0, 240, 960, and 2880 min. The fractographic examination of the as-quenched sheet reveals that the fracture surface is covered with dimples and flat surfaces, indicating a mixture of ductile and brittle fractures. However, the ductility value of the as-quenched samples was high (31.1%). Certainly, with this high amount of ductility, the fracture surface should not show flat surfaces. The presence of flat surfaces on the fracture

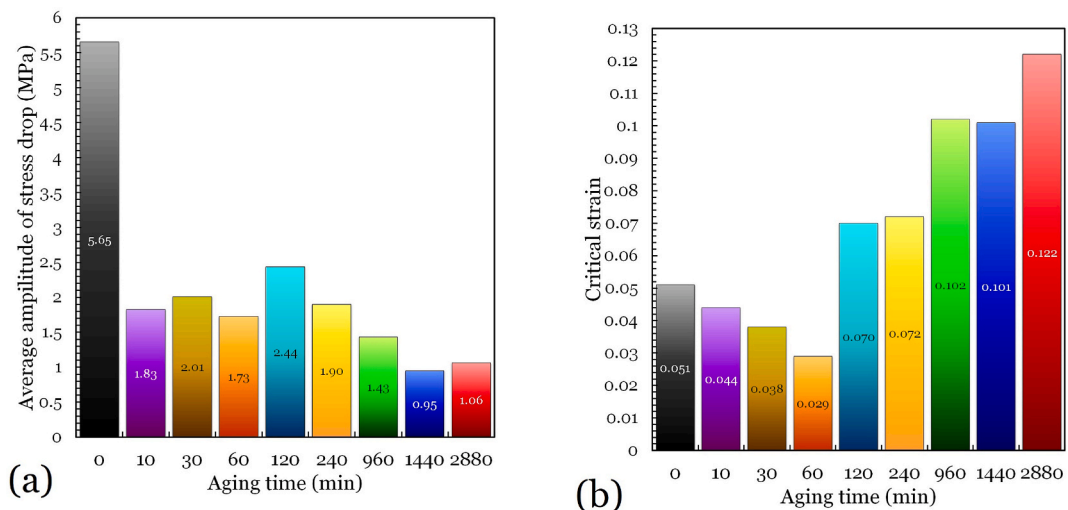


Fig. 10. (a) Average amplitude and (b) critical strain of stress drop of all samples.

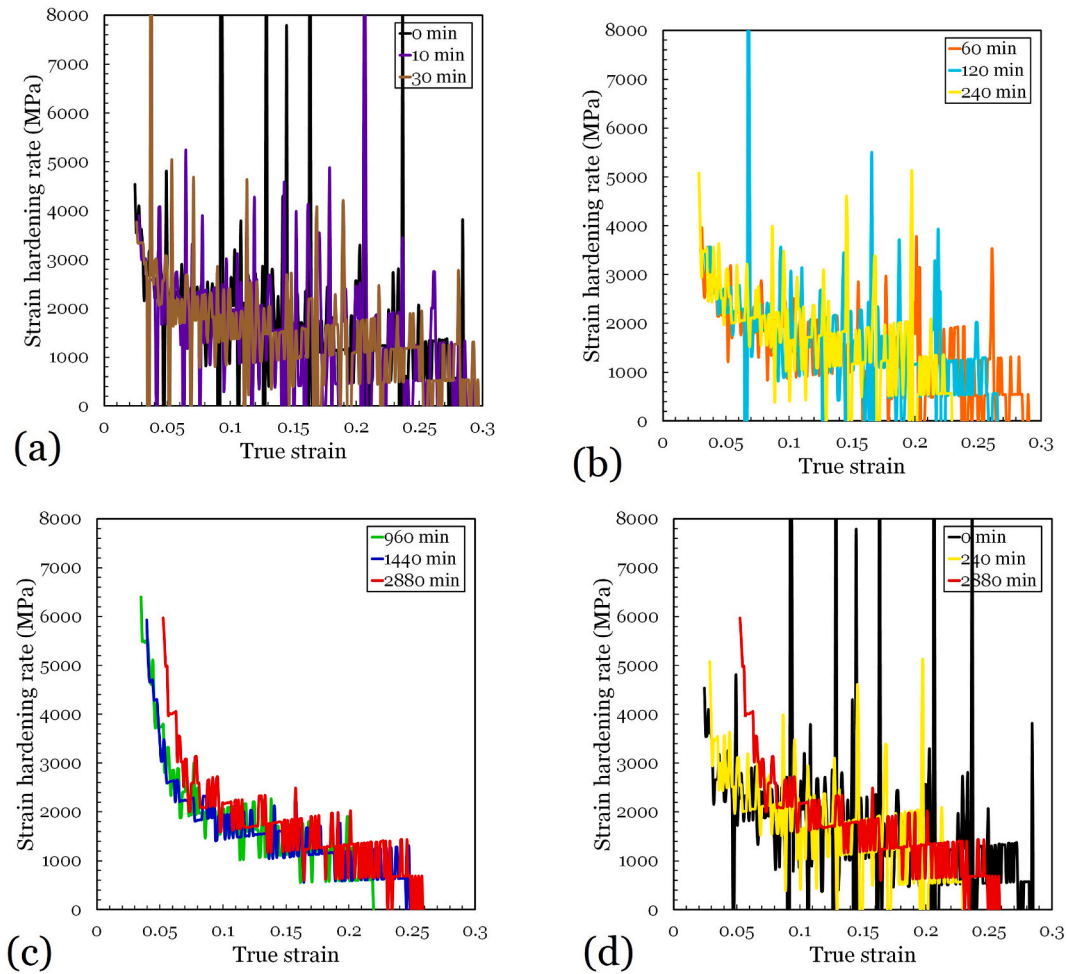


Fig. 11. Work hardening rate ($\theta = d\sigma/d\varepsilon$) of the sheets after (a) 0, 10, 30, (b) 60, 120, 240, (c) 960, 1440, 2880, (d) 0, 240, 2880 min of natural re-aging time.

surface of the as-quenched alloy can be attributed to the occurrence of severe serrations during the tensile deformation. With increasing the natural re-aging time to 240 min, the fraction of flat surfaces is decreased and the fraction of dimples is increased. Considering the lower ductility of the re-aged sample for 240 min (24.2%) compared to the as-quenched sample, it was expected that flat surfaces would be more in the re-aged sample for 240 min. This contradiction is related to the weakening of the Portevin Le-Chatelier effect in the re-aged sample for 240 min as displayed in Figs. 9 and 10. An important point in the fracture surfaces of the re-aged sheets for 0 and 240 min is that very few $\text{Al}_7\text{Cu}_2\text{Fe}$ particles are visible. This result can be related to the lack of an effective load transfer mechanism caused by Portevin Le-Chatelier instability. In other words, more Portevin Le-Chatelier instability causes the formation of more flat surfaces and as a result more brittle fracture of the aluminum matrix, and the load transfer mechanism cannot work properly. With further increasing the natural re-aging time to 960 min, the fracture surface appearance is predominately ductile with the formation of many dimples. After natural re-aging for 960 min, the number of dimples is remarkably increased and flat surfaces are not observed on the fractographs. As can be seen in Fig. 12(e), the number of $\text{Al}_7\text{Cu}_2\text{Fe}$ particles visible at the fracture surface of the re-aged sample for 960 min increases significantly. Also, most of the $\text{Al}_7\text{Cu}_2\text{Fe}$ particles have fractured. These results are due to effective load transfer from the aluminum matrix to the $\text{Al}_7\text{Cu}_2\text{Fe}$ particles caused by the significant weakening of the Portevin Le-Chatelier instability. Finally, by increasing the re-aging time to 2880 min, the number of dimples is increased again, which is indicative of large plastic deformation before failure (ductility of 28.9% without Portevin Le-Chatelier instability). As can be observed in Fig. 12(h), the size of the dimples decreases in the re-aged sample for 2880 min and parts of the fracture surface include very fine dimples as indicated by orange arrows. Also, there are very small precipitates at the bottom of some dimples as displayed by yellow arrows in Fig. 12(h). The remarkable increase in the tensile strength of the re-aged sample for 960 and 2880 min can be also related to the effective load-bearing hardening (direct strengthening), which causes a proper load transfer from soft aluminum to hard $\text{Al}_7\text{Cu}_2\text{Fe}$ particles. It can be concluded that the strengthening of the natural re-aged sample for 2880 min is a result of a synergistic effect of precipitation hardening due to the formation of θ'' , S'' , θ' , and S' phases, suppression of Portevin Le-Chatelier instability, and highly efficient load transfer from alpha-aluminum to $\text{Al}_7\text{Cu}_2\text{Fe}$.

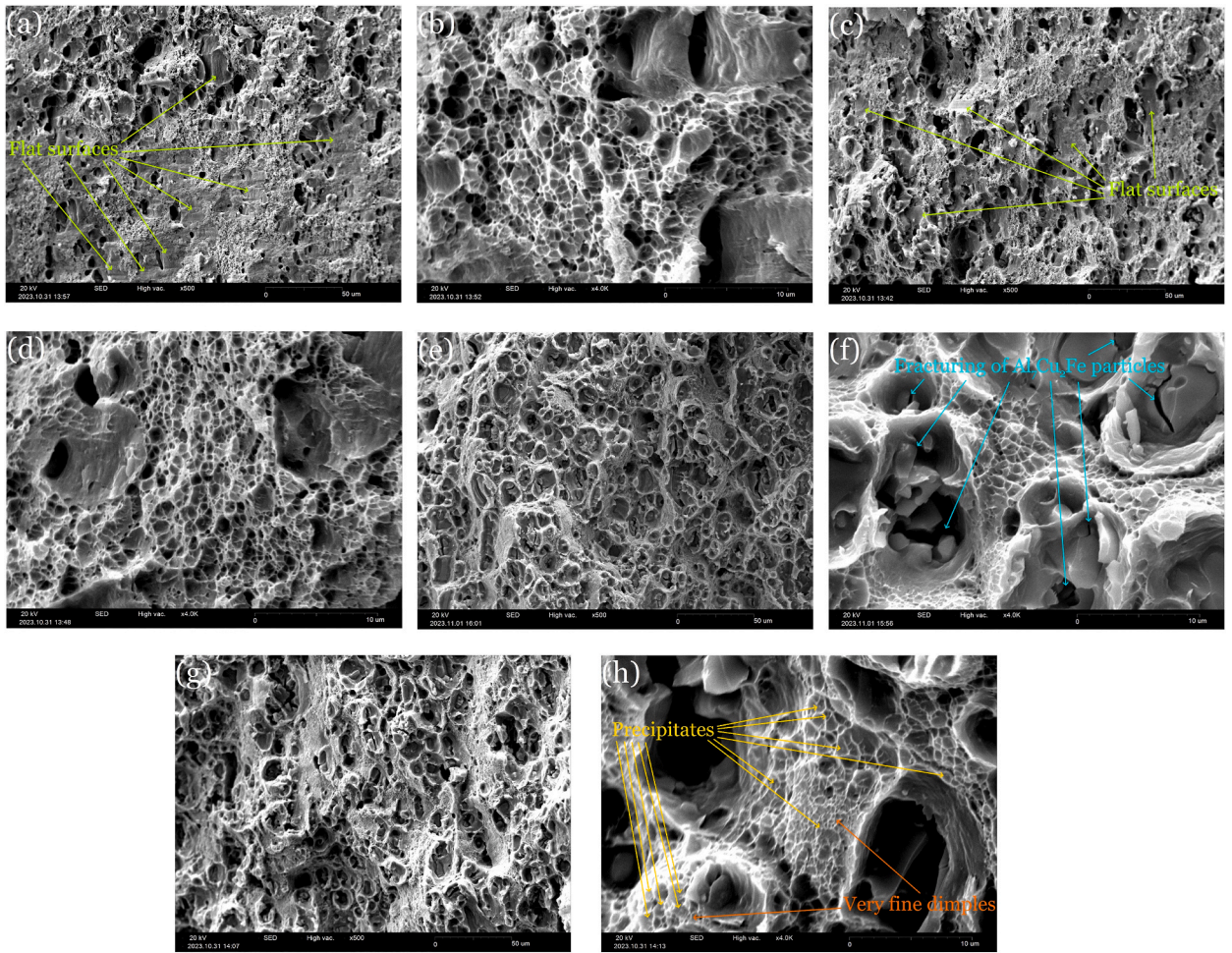


Fig. 12. Fracture surfaces of the natural re-aged sheets for (a,b) 0, (c,d) 240, (e,f) 960, and (g,h) 2880 min.

Based on the results obtained from this research, the AA2024 sheet produced by natural re-aging showed excellent strength and ductility. In order to use the alloy produced by natural re-aging (for 1440 or 2880 min), two methods are proposed, which can be seen in Fig. 13. In the first method, the T351 process in the AA2024 sheet production factory and natural re-aging treatment should be conducted in the factory of the finished product (the product in the last stage of manufacturing company's product process). Therefore, during the transportation of the AA2024 sheets from the sheet production factory to the final product factory, there is no need to keep the sheets in cryogenic conditions. But in the second method, both steps must be performed at the AA2024 sheet production factory. As

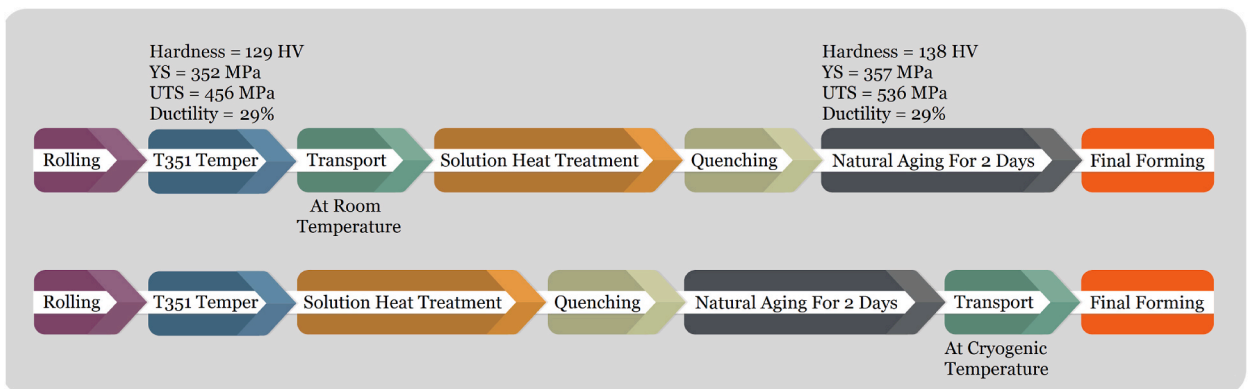


Fig. 13. Two proposed processes with natural re-aging.

a result, during the transportation of the sheets from the sheet production factory to the final product factory, the re-aged AA2024 sheets must be in a cryogenic condition because further natural re-aging is inevitable.

4. Conclusion

1. Grain growth occurred in the microstructures of the natural re-aged sample and a large number of Al₇Cu₂Fe particles were located inside the alpha grains.
2. At the re-aging time of 1440 min, the peaks of XRD were shifted strongly to the right due to the formation of θ'' , S'', θ' , and S'. The precipitation rate was high in the AA2024 alloy during natural aging. With increasing the re-aging time, texture parameters remained almost unchanged.
3. The hardness increased slowly within the first 60 min, then enhanced rapidly between 60 and 2880 min, and finally became stable at around 139 HV between 2880 and 11520 min.
4. When the natural re-aging time increased from 240 to 2880 min, the strengthening trended speed up, viz, the yield strength increased from 226.6 to 357.3 MPa, and the ultimate tensile strength enhanced from 452.2 to 535.5 MPa.
5. Compared to the as-received sample (T351 temper), the tensile strength of the re-aged sheet improved from 455.5 to 535.5 MPa, the ductility remained unchanged, and the hardness increased from 128.8 to 138.2 HV, which was owing to the acceleration of the precipitation caused by the presence of high-content Al₇Cu₂Fe particles in the interior of the alpha-aluminum grains in the natural re-aged sample.
6. The Portevin-Le Chatelier instability of AA2024 alloy was effectively postponed after natural re-aging. With increasing the natural re-aging time, the work hardening rate of the AA2024 alloy increased.
7. The strengthening of the natural re-aged sample for 2880 min was a result of a synergistic effect of precipitation hardening due to the formation of precipitates, elimination of Portevin Le-Chatelier instability, and highly efficient load transfer from alpha-aluminum to Al₇Cu₂Fe.
8. To use the AA2024 alloy produced by natural re-aging for 1440 or 2880 min, two methods were proposed.

Additional information

No additional information is available for this paper.

Data availability

All data included in this study are available upon request by contact with the corresponding author.

CRedit authorship contribution statement

Farima Haghdad: Writing – original draft, Resources, Investigation. **Roohollah Jamaati:** Writing – review & editing, Supervision, Methodology. **Seyed Jamal Hosseinipour:** Writing – review & editing, Supervision, Methodology.

Declaration of competing interest

The authors declare that they have no known competing financial interests or personal relationships that could have appeared to influence the work reported in this paper.

References

- [1] I. Polmear, D. StJohn, J.-F. Nie, M. Qian, *Light Alloys: Metallurgy of the Light Metals*, Butterworth-Heinemann, 2017.
- [2] B. Klober, K. Maier, T.E.M. Staab, Natural ageing of Al–Cu–Mg revisited from a local perspective, *Materials Science and Engineering: A* 528 (7) (2011) 3253–3260.
- [3] M.R. Roodgari, R. Jamaati, Ultrahigh-temperature aging response of asymmetrically cold-rolled AA2024 alloy, *CIRP Journal of Manufacturing Science and Technology* 39 (2022) 232–243.
- [4] M.R. Roodgari, R. Jamaati, A technique to achieve an excellent strength-ductility balance in AA2024 alloy, *Arch. Civ. Mech. Eng.* 23 (1) (2022) 12.
- [5] S. Dai, Z. Bian, W. Wu, J. Tao, L. Cai, M. Wang, C. Xia, H. Wang, The role of Sn element on the deformation mechanism and precipitation behavior of the Al–Cu–Mg alloy, *Materials Science and Engineering: A* 792 (2020) 139838.
- [6] A. Guinier, Structure of age-hardened aluminium-copper alloys, *Nature* 142 (3595) (1938) 569–570.
- [7] G.D. Preston, LXXIV. The diffraction of X-rays by an age-hardening alloy of aluminium and copper. The structure of an intermediate phase, *Dublin Phil. Mag. J. Sci.* 26 (178) (1938) 855–871.
- [8] H.K. Hardy, The ageing characteristics of binary Aluminium-Copper Alloys, *J. Inst. Met.* 79 (1951) 321–369.
- [9] A. Cochar, K. Zhu, S. Joulie, J. Douin, J. Huez, L. Robbiola, P. Sciau, M. Brunet, Natural aging on Al-Cu-Mg structural hardening alloys – investigation of two historical duralumins for aeronautics, *Materials Science and Engineering: A* 690 (2017) 259–269.
- [10] F. Lotter, D. Petschke, F. De Geuser, M. Elsayed, G. SEXTL, T.E.M. Staab, In situ natural ageing of Al-Cu-(Mg) alloys: the effect of in and Sn on the very early stages of decomposition, *Scripta Mater.* 168 (2019) 104–107.
- [11] I. Kim, M. Song, J. Kim, S. Hong, Effect of added Mg on the clustering and two-step aging behavior of Al–Cu alloys, *Materials Science and Engineering: A* 798 (2020) 140123.
- [12] R. Ivanov, A. Deschamps, F. De Geuser, Clustering kinetics during natural ageing of Al-Cu based alloys with (Mg, Li) additions, *Acta Mater.* 157 (2018) 186–195.
- [13] M. Liu, R. Zheng, J. Li, C. Ma, Achieving ultrahigh tensile strength of 1 GPa in a hierarchical nanostructured 2024 Al alloy, *Materials Science and Engineering: A* 788 (2020) 139576.

- [14] J.A. Österreicher, D. Nebeling, F. Grabner, A. Cerny, G.A. Zickler, J. Eriksson, G. Wikström, W. Suppan, C.M. Schlögl, Secondary ageing and formability of an Al-Cu-Mg alloy (2024) in W and under-aged tempers, *Mater. Des.* 226 (2023) 111634.
- [15] B. Decreus, A. Deschamps, F. De Geuser, P. Donnadieu, C. Sigli, M. Weyland, The influence of Cu/Li ratio on precipitation in Al-Cu-Li-x alloys, *Acta Mater.* 61 (6) (2013) 2207–2218.
- [16] S. Manna, H. Chan, A. Ghosh, T. Chakrabarti, S.K.R.S. Sankaranarayanan, Understanding and control of Zener pinning via phase field and ensemble learning, *Comput. Mater. Sci.* 229 (2023) 112384.
- [17] A. Rollett, G.S. Rohrer, J. Humphreys, *Recrystallization and Related Annealing Phenomena*, Elsevier Science, 2017.
- [18] X.W. Fang, H. Xiao, K. Marthinsen, A. Belyakov, X.Y. Fang, K. Huang, Tailoring microstructure and texture of annealed Al-Mn alloy through the variation of homogenization and prior cold deformation strain, *Mater. Char.* 166 (2020) 110438.
- [19] Y. Song, W. Du, L. Zhao, L. Zeng, W. Liu, Y. Chen, B. Zhu, X. Zhang, X. Ding, The coupling influences and corresponding mechanisms of high efficiency thermal-magnetic treatments on the dimensional stability of Al-Cu-Mg alloy, *J. Alloys Compd.* 928 (2022) 167187.
- [20] Y. Song, Q. Zhang, W. Du, X. Ding, Y. Chen, W. Liu, Effect of thermal-cold cycling treatment on microstructural stability of Al-Cu-Mg alloy hemispherical component, *J. Alloys Compd.* 969 (2023) 172388.
- [21] W. Mo, C. Tang, P. Deng, Z. Ouyang, B. Luo, Z. Bai, Effect of trace Zn addition on microstructure and corrosion behavior of AA2024 under different aging treatments, *Mater. Char.* 195 (2023) 112440.
- [22] I. Zuiko, R. Kaibyshev, Aging behavior of an Al-Cu-Mg alloy, *J. Alloys Compd.* 759 (2018) 108–119.
- [23] H. Wang, Y. Li, G. Xu, J. Li, T. Zhang, B. Lu, W. Yu, Y. Wang, Y. Du, Effect of nano-TiC/TiB₂ particles on the recrystallization and precipitation behavior of AA2055-TiC+TiB₂ alloys, *Materials Science and Engineering: A* 871 (2023) 144927.
- [24] A.M. Korsunsky, A.I. Salimon, I. Pape, A.M. Polyakov, A.N. Fitch, The thermal expansion coefficient of mechanically alloyed Al-Cu-Fe quasicrystalline powders, *Scripta Mater.* 44 (2) (2001) 217–222.
- [25] M.J. Starink, B. Milkereit, Y. Zhang, P.A. Rometsch, Predicting the quench sensitivity of Al-Zn-Mg-Cu alloys: a model for linear cooling and strengthening, *Mater. Des.* 88 (2015) 958–971.
- [26] M. Zhang, J. Wang, B. Wang, C. Xue, X. Liu, Quantifying the effects of Sc and Ag on the microstructure and mechanical properties of Al-Cu alloys, *Materials Science and Engineering: A* 831 (2022) 142355.
- [27] P. Jin, Y. Liu, F. Li, Q. Sun, Realization of synergistic enhancement for fracture strength and ductility by adding TiC particles in wire and arc additive manufacturing 2219 aluminium alloy, *Compos. B Eng.* 219 (2021) 108921.
- [28] X. Zhang, L. Zhang, Z. Zhang, X. Huang, Effect of solute atoms segregation on Al grain boundary energy and mechanical properties by first-principles study, *Mech. Mater.* 185 (2023) 104775.
- [29] C.H. Wu, H. Li, T.J. Bian, C. Lei, L.W. Zhang, Natural aging behaviors of Al-Cu-Li alloy: PLC effect, properties and microstructure evolution, *Mater. Char.* 184 (2022) 111694.
- [30] S.-Y. Lee, C. Takushima, J.-i. Hamada, N. Nakada, Macroscopic and microscopic characterizations of Portevin-LeChatelier effect in austenitic stainless steel using high-temperature digital image correlation analysis, *Acta Mater.* 205 (2021) 116560.
- [31] A. Chatterjee, A. Sarkar, P. Barat, P. Mukherjee, N. Gayathri, Character of the deformation bands in the (A+B) regime of the Portevin-Le Chatelier effect in Al-2.5%Mg alloy, *Materials Science and Engineering: A* 508 (1) (2009) 156–160.
- [32] N. Nayan, S.V.S. Narayana Murty, R. Sarkar, A.K. Mukhopadhyay, S. Ahlawat, S.K. Sarkar, M.J.N.V. Prasad, I. Samajdar, The anisotropy of serrated flow behavior of Al-Cu-Li (AA2198) alloy, *Metall. Mater. Trans.* 50 (11) (2019) 5066–5078.
- [33] J. Kang, D.S. Wilkinson, M. Jain, J.D. Embury, A.J. Beaudoin, S. Kim, R. Mishra, A.K. Sachdev, On the sequence of inhomogeneous deformation processes occurring during tensile deformation of strip cast AA5754, *Acta Mater.* 54 (1) (2006) 209–218.
- [34] M. Cui, S.H. Kayani, H.-W. Kim, J.-H. Lee, The role of prestraining on mechanical properties and microstructure of preaged AA 6016 Al-Mg-Si sheets, *J. Alloys Compd.* 960 (2023) 170681.
- [35] Y.-S. Lee, D.-H. Koh, H.-W. Kim, Y.-S. Ahn, Improved bake-hardening response of Al-Zn-Mg-Cu alloy through pre-aging treatment, *Scripta Mater.* 147 (2018) 45–49.
- [36] M. Liu, J. Chen, Y. Lin, Z. Xue, H.J. Roven, P.C. Skaret, Microstructure, mechanical properties and wear resistance of an Al-Mg-Si alloy produced by equal channel angular pressing, *Prog. Nat. Sci.: Mater. Int.* 30 (4) (2020) 485–493.